IEEE Access
Multidisciplinary | Rapid Review | Open Access Journal

Received April 1, 2021, accepted April 11, 2021, date of publication April 21, 2021, date of current version April 30, 2021.

Digital Object Identifier 10.1109/ACCESS.2021.3074626

Auto-Tuning of DC-DC Buck Converters Through the Modified Relay Feedback Test

AHMED SHEHADA[1], YAN YAN[1], ABDUL R. BEIG[2], (Senior Member, IEEE), AND IGOR BOIKO[1], (Senior Member, IEEE)

[1]Department of Electrical Engineering and Computer Science, Khalifa University, Abu Dhabi, United Arab Emirates
[2]Advanced Power and Energy Center, Department of Electrical Engineering and Computer Science, Khalifa University, Abu Dhabi, United Arab Emirates

Corresponding author: Igor Boiko (igor.boiko@ku.ac.ae)

This work was supported by the Khalifa University Research Grant CIRA-2018-104.

ABSTRACT This paper presents the design and application of the modified relay feedback test (MRFT) auto-tuning method to the PID voltage-mode control of dc-dc buck converters. The proposed method, which also includes a set of tuning rules, does not require knowledge of the converter or load parameters, and produces a controller with near-optimal dynamic performance for virtually any dc-dc buck converter. The proposed MRFT auto-tuning also guarantees a specified phase margin. An important feature of the MRFT auto-tuning is that it is non-complex and thus practical, consisting of a simple test stage and a quick tuning stage. In the test stage oscillations are excited using the MRFT algorithm, and the frequency and amplitude of these oscillations are measured. In the tuning stage, these measurements are used with the pre-designed tuning rules to calculate PID controller parameters. The designed MRFT auto-tuning is evaluated experimentally by using it to auto-tune four different dc-dc buck converter designs, where in each case parameters of the converter are unknown to the auto-tuning algorithm. The experimental results show good performance of the MRFT auto-tuned controller in all cases. A mathematical proof that the MRFT auto-tuning guarantees a specified phase margin is also provided.

INDEX TERMS Auto-tuning, dc-dc converters, digital control, modified relay feedback test.

I. INTRODUCTION

The constant evolution of digital controllers with improved speeds and lower cost-to-performance ratio has led to their increased adoption in switching power converters, where analog controllers used to be prevalent [1]. Unlike its analog counterpart, the digital controller can be re-tuned as needed, and does not suffer from controller parameter variation due to component ageing. Digital controllers can also implement more complex control algorithms that can achieve various performance goals. This has encouraged more research on the auto-tuning of digitally-controlled dc-dc converters [2]–[23]. Auto-tuning refers to the automatic online tuning of a controller upon a user/event prompt or at pre-set intervals.

A. BENEFITS OF AUTO-TUNING IN POWER CONVERTERS

Commercial converters, especially those manufactured in volume, typically have their controller tuned based on an estimated analytical model that uses nominal component values, as it is not feasible to measure the actual value of the components for every converter in the line. Analytical models used for this purpose typically represent only the major dynamics of a system, neglecting minor dynamics such as smaller delays and non-linearities, and often disregarding some or all of the parasitic effects. Auto-tuning on the other hand is performed online on the actual converter after deployment in an application environment, and so it captures the actual component values, thereby eliminating errors related to component tolerance, ageing, and parasitic effects. Auto-tuning also accounts for the actual value of the connected load, and includes the influence of the input capacitance of a next-stage converter.

Auto-tuning methods may be categorized into parametric and non-parametric ones. All auto-tuning methods begin with a test to excite the system's dynamics. A system identification may then be performed, and the controller is tuned based on the identified system. In this case, the auto-tuning is called parametric. But if system identification is skipped and tuning is done immediately after the test, the auto-tuning is referred to as non-parametric. The present paper proposes

The associate editor coordinating the review of this manuscript and approving it for publication was Yuh-Shyan Hwang.

a non-parametric auto-tuning of a digitally-controlled dc-dc buck converter that can be used on a converter with virtually any combination of filter inductor (L), filter capacitor (C), resistive load (R_o), and switching frequency (f_{sw}) values. The proposed auto-tuning consists of a short test stage in which oscillations are excited under certain conditions, followed by a tuning stage in which the measured amplitude and frequency of the excited oscillations are used in pre-designed tuning rules to obtain near-optimal PID parameters. A review of related literature is first given before the proposed auto-tuning method is explained.

B. REVIEW OF DC-DC CONVERTER AUTO-TUNING METHODS

In [2]–[6], the test stage of the auto-tuning uses a pseudo-random binary sequence (PRBS) to excite the converter's dynamics. The PRBS is a digital approximation of white noise that is easy to generate and frequency-rich. The PRBS signal is added as a small perturbation to the steady-state duty-cycle input. The cross-correlation of the input PRBS and the excited output, followed by a Discrete Fourier Transform (DFT), provides the converter's frequency response (FR) in discrete form (as real and imaginary data). In [2], the PRBS test is applied to a forward dc-dc converter, and the obtained FR data is used to perform full parametric identification of the system using a least-squares method. A direct digital design approach is then used to tune the controller to achieve the desired closed-loop response. While the test stage duration is not long, the online system identification stage involves minimizing a cost function, which could take appreciable time. In [3] the FR data obtained after exciting the buck converter with PRBS is used in a multi-stage procedure to directly tune the controller without identifying the system's parameters. Tuning goals in [3] include obtaining the specified phase margin, achieving high bandwidth, and limiting output voltage perturbations during the test stage. Work in [3] is further extended in [4] where it is applied to a buck converter with different damping levels, as well as to a boost converter in both continuous and discontinuous conduction modes (CCM and DCM). While good controller designs are achieved in [3], [4], a disadvantage is that tuning is done in multiple stages of several iterations each. This may not be highly reliable when it comes to practical application. It is also noted that in [3], [4], the system operates in open-loop mode during the test stage. In [7], the classic chirp signal is used for excitation, and a DFT is used to obtain the system's FR. However, the test stage duration is considerably long.

Another important class of dc-dc converter auto-tuning is that based on the relay feedback test (RFT) [24]. The RFT is performed by replacing the controller with a relay and operating the system in closed-loop. The relay can be operated around the steady-state duty-cycle, D, such that when the relay is ON a small perturbation (h) is added to D, and when relay is OFF h is subtracted from D. The relay function of the RFT is described by the following equation, where $u(t)$ is the control command produced by the relay, and $e(t)$ is the error signal given by the difference between the reference $r(t)$ and the output $y(t)$.

$$u(t) = \begin{cases} D + h, & e(t) > 0 \\ D - h, & e(t) < 0 \end{cases} \tag{1}$$

The RFT produces oscillations at the system's phase crossover ($-180°$) frequency; the amplitude and time period measurements of the excited oscillations may then be used for tuning the controller. In [8] these measurements are used with the Ziegler and Nichols (Z-N) tuning rules to auto-tune the PID controller of a dc-dc buck converter. However, the Z-N rules do not allow for the specification of the gain or phase margin, and stability itself is not guaranteed – except when a proportional-only controller is used. In [9], a modified RFT-based auto-tuning is applied to a dc-dc buck converter. An integrator is placed in series with the relay to add an extra 90° phase shift, which excites oscillations at approximately the LC resonant frequency of the converter. Tuning is not done using tuning rules, but rather through an iterative procedure. First, one zero of the PID controller is placed at the LC resonant frequency, while the second zero is iteratively tuned to meet the desired phase margin. Finally, the proportional gain is iteratively tuned to achieve the desired bandwidth. A disadvantage of this method is the requirement for several tuning stages, with some involving iterations, which may not be favorable in practical application. Also, since the first stage excites the system at the LC resonant frequency where the converter's gain is highest, tuning is performed at a voltage below the nominal (during the soft-start), which means that the auto-tuning can only be performed during startup and not when the converter is in normal operation. This is another practical limitation of the auto-tuning in [9]. A modified version of this work is presented in [10], where only time-period measurements of the RFT oscillations are used in order to avoid errors associated with amplitude measurements. However, the tuning part of the method still involves several stages that include iterations. Similar work is reported in [3] for a dc-dc buck converter with a wide range of capacitive loads.

Also based on RFT, in [11] sustained oscillations are excited in a dc-dc buck converter by reducing the resolution of the digital PWM, which imitates the relay action. Integral-only control is maintained during the test stage. System identification is then performed, and a stored lookup table is used to select the controller coefficients. Though tuning is simpler than methods in [3], [4], [9], and [10], a tradeoff exists between the size of the stored lookup table and the number of possible discrete control laws. In [12] a parametric approach is adopted for the auto-tuning of a dc-dc buck converter. Using Fourier analysis of the RFT results, the buck converter transfer function is identified. Tuning rules developed offline are then used to calculate controller parameters. However, it is required to measure the time it takes from the moment of applying the relay until sustained oscillations start. Such

parameter may be difficult to measure experimentally with reasonable accuracy, and this work has not been verified experimentally. In [13] another parametric tuning based on the RFT is reported, where a PID controller is tuned based on an identified model, with the goal of achieving a certain phase margin. However, both the identification and PID parameter calculation are seemingly done offline, and it is not clear whether the identification and PID tuning are simple enough to be easily automated.

Different from auto-tuning, continuous adaptive tuning is suggested in [14], [15]. Small perturbations are injected digitally on top of the duty-cycle input while the system is operating in closed-loop, and PID parameters are continuously adjusted to meet design goals such as bandwidth and phase margin. Advantages of such approach include maintaining regulation during tuning, and continuous adaptation to system changes. Experimental application of such scheme to a dc-dc buck converter operating in CCM is reported in [14], and for CCM and DCM operation in [15]. A disadvantage of such adaptive methods, as pointed out in [4], is the requirement of some prior knowledge of the converter to ensure that parameter update rates do not lead to instability. A major challenge also is handling the situation where the desired closed-loop performance cannot be achieved. Other auto-tuning methods, using various test/tuning techniques and applied to different dc-dc converters, are found in [16]–[23].

As seen from the above, methods reported in the literature vary widely in terms of technique, duration, etc. The RFT-based method in [8] has very simple test and tuning, but the tuning is simplistic and yields a moderate performance. Methods such as [2]–[4] and [9], [10] report good tuning, but they either take significant time to auto-tune, and/or have some level of complexity in the tuning. A practical auto-tuning should have short and simple test and tuning stages. This may be achieved by using general knowledge of the system to develop tuning rules offline, which would reduce the online tuning effort, thus making the auto-tuning faster and less complex. While references [12] and [13] adopt such approach, they involve computations that are quite complex. Also as mentioned earlier [12] is not experimentally verified, and for [13] it is not clear whether the approach can be easily automated. The present work uses the modified relay feedback test (MRFT) [25] auto-tuning method, which is based on a powerful *coordinated test and tuning* concept. With a single set of pre-designed tuning rules (being the major contribution of this work), the presented method may be used for the auto-tuning of a wide range of designs of a digital PID-controlled dc-dc buck converter. Advantages of the MRFT auto-tuning method are: (i) the auto-tuning is simple, fast, and reliable; (ii) it guarantees a certain specified gain or phase margin; (iii) it provides near-optimal dynamic performance; (iv) it does not require knowledge of any of the converter or load parameters; (v) has a minimal impact on the converter's operation; and (vi) it is a small program, so in most cases it can be easily added to the existing digital controller.

MRFT auto-tuning has been theoretically demonstrated on process systems such as flow, level, and temperature loops [25]. In this work it is applied to a switching power converter, which is more challenging and unique due to the fast dynamics of the system and the presence of PWM. The main contributions of the present work are:

1. Design and application of the MRFT auto-tuning to dc-dc buck converters. This includes producing a test parameter and coefficients of the tuning rules that are optimal for the class of dc-dc buck converters. This ensures near-optimal dynamic performance for any dc-dc buck converter within a wide range of dc-dc buck converter designs; the range of designs is specified in section III-B.
2. Implementation of the MRFT on a dc-dc switching buck power converter, which is non-trivial use of the MRFT, due to the use of PWM in the converter.
3. Experimental results for four different buck converter test designs to verify that the designed MRFT auto-tuning with the proposed optimal tuning rules can be successfully applied to different buck converter designs without knowledge of any of the converter's parameters.
4. Mathematical proof that the specified phase margin is guaranteed by the MRFT auto-tuning method with the proposed tuning rules.

Section II gives an overview of the MRFT auto-tuning method and provides proof that the method guarantees the specified phase margin. Section III explains the procedure used to develop the proposed optimal tuning rules, which is done through a two-layer optimization with the objective of obtaining near-optimal dynamic performance. Section IV provides experimental results for the MRFT auto-tuned controller and compares its performance to that of a non-auto-tunable controller designed optimally with full knowledge of the system. Finally, section V provides concluding remarks.

II. OVERVIEW OF THE MRFT AUTO-TUNING METHOD

The MRFT auto-tuning is a PID controller tuning method consisting of a simple test stage and a quick tuning stage. A PID controller of the following form is used, where K_c is the proportional gain, T_i the integral time and T_d the derivative time.

$$W_c(s) = K_c\left(1 + \frac{1}{T_i s} + T_d s\right) \tag{2}$$

It is usually impossible to design a single controller to fit a wide range of converter designs, since different L, C, R, and f_{sw} would require significantly different PID parameters. But it is indeed possible to design tuning rules to fit a wide range, which is achieved in this work. The format of the PID tuning rules of the MRFT auto-tuning method are as follows, where coefficients c_1, c_2, and c_3 are positive constants [25].

$$K_c = c_1 K_u, \quad T_i = c_2 T_u, \quad T_d = c_3 T_u \tag{3}$$

K_u and T_u are outputs of the test stage that will be explained shortly. The coefficients of the tuning rules (c_1, c_2, c_3), as well as a test parameter (β), must be selected (i.e. designed) before the online MRFT auto-tuning is conducted. However, it is helpful to have an understanding of the online MRFT auto-tuning process (i.e. the test and tuning stages) before the selection process of the set (β, c_1, c_2, c_3) is discussed. Finding the optimal set of (β, c_1, c_2, c_3) is addressed later in section III.

A. DESCRIPTION OF TEST STAGE OF THE MRFT AUTO-TUNING

The test stage of the MRFT auto-tuning method is performed by replacing the PID controller with a modified relay and running the system in closed-loop, as shown in Fig. 1 (a), where $W_p(s)$ is the plant to be controlled. The modified relay is described by the following discontinuous control [25]:

$$u(t) = \begin{cases} h, \text{ if } & e(t) \geq -\beta e_{min} \\ & \text{or} \\ & \{e(t) \geq -\beta e_{max} \;\&\; u(t-) = h\} \\ -h, \text{ if } & e(t) \leq -\beta e_{max} \\ & \text{or} \\ & \{e(t) \leq -\beta e_{min} \;\&\; u(t-) = -h\} \end{cases} \tag{4}$$

where $0 < \beta < 1$, and e_{max} and e_{min} represent the last maximum and last minimum of the error signal $e(t)$, respectively. $u(t-)$ is the control output immediately prior to time t. Fig. 1 (b) provides a diagrammatic illustration of the test stage of the MRFT auto-tuning method. The test is started with e_{max} and e_{min} set to zero. Since $u(t)$ is always non-zero, oscillations start to develop in $y(t)$ and $e(t)$. Every time a minimum (e_{min}) or maximum (e_{max}) is recorded, the corresponding switching condition ($-\beta e_{max}$ or $-\beta e_{min}$) for the upcoming half-cycle is updated. The MRFT thus acts as a hysteretic relay with a dynamically-changed hysteresis value that depends on the amplitude of oscillations (e_{max} or $-e_{min}$), which typically stabilizes after a few transient cycles such that $e_{max} = -e_{min}$.

In the context of the dc-dc converter, a straightforward method to run the test is to disable the pulse-width modulation (PWM) and let the MRFT relay directly control the converter switches, so that when the relay is ON, the main switch is turned ON, and when the relay is OFF, the main switch is turned OFF. But since the MRFT frequency is typically much lower than the PWM frequency, switching at the MRFT frequency will result in an increased ripple in both the inductor current and the output voltage. The present work adopts a more appropriate approach of double-modulation, where the PWM is still maintained during the test stage, and the MRFT modulation is only superposed on top of it. This is done by setting the relay output, $u(t)$, to either $D + h$ (when the relay is ON) or $D - h$ (when the relay is OFF), where D is the nominal duty cycle output by the controller at steady-state just prior to application of the MRFT, and where h is a small perturbation (e.g. 3% of D).

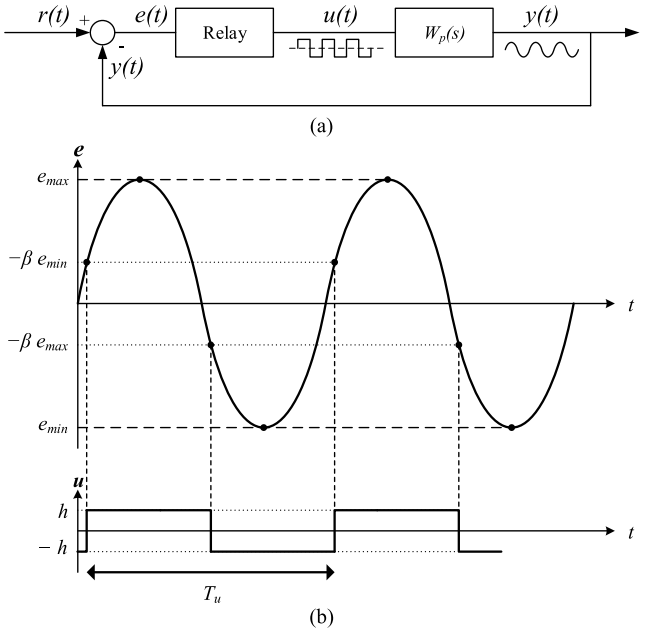

FIGURE 1. Block diagram and illustrative waveforms of the MRFT algorithm.

In such approach, the MRFT oscillations appear superposed on top of the nominal output voltage. In terms of gate pulses, the MRFT manifests as a series of slightly wider PWM pulses corresponding to the $D+h$ duty-cycle and lasting for $T_u/2$, followed by a series of slightly narrower PWM pulses corresponding to the $D-h$ duty-cycle and also lasting for $T_u/2$, where T_u is the time period of the MRFT oscillations. The advantage of the adopted approach is that the converter maintains the switching frequency it was designed for even during the test stage, thus maintaining an acceptable level of ripple. This minimizes the impact of the MRFT auto-tuning on the converter, making it possible to take place even during normal operation (in most applications). The modified relay in such approach is expressed in (5) below. Compared to (4), the relay of (5) includes D. Also, the relay in (5) has been modified to allow for both positive and negative values for β, whereas (4) could only be used for positive values of β.

$$u(t) = \begin{cases} D+h, \text{ if } & \{e(t) \geq -\beta e_{min} \;\&\; u(t-) = D-h\} \\ & \text{or} \\ & \{e(t) \geq -\beta e_{max} \;\&\; u(t-) = D+h\} \\ D-h, \text{ if } & \{e(t) \leq -\beta e_{max} \;\&\; u(t-) = D+h\} \\ & \text{or} \\ & \{e(t) \leq -\beta e_{min} \;\&\; u(t-) = D-h\} \end{cases} \tag{5}$$

Let the amplitude of the MRFT oscillations once they have stabilized be $a_0 = e_{max} = -e_{min}$. Also let $\Omega_0 = 2\pi/T_u$ be the measured frequency of oscillations (in *rad/s*). The term K_u in (3), called ultimate gain, is calculated as follows [25]:

$$K_u = \frac{4h}{\pi a_0} \tag{6}$$

This completes the test stage. For improved accuracy, T_u and a_0 are best computed as an average over a few oscillation cycles. The tuning stage is then simply to calculate K_u using (6), then calculate the updated PID parameters using (3).

B. CONDITIONS FOR GUARANTEEING SPECIFIED PHASE MARGIN

The theory of the MRFT auto-tuning method states that selecting (β, c_1, c_2, c_3) as per the following constraints would guarantee the specified phase margin, φ_m, for any arbitrary system [25], [26].

$$\begin{aligned} c_1\sqrt{1+\xi^2} &= 1 \\ \beta &= \sin\left(\phi_m - \tan^{-1}\xi\right) \\ \text{, where } \xi &= 2\pi c_3 - \frac{1}{2\pi c_2} \end{aligned} \tag{7}$$

A mathematical proof of this, not previously presented, is given here. The harmonic balance, described by the equation below, should be satisfied at frequency Ω_0 (i.e. when the oscillations have stabilized) [27]:

$$W_p\left(j\Omega_0\right) N\left(a_0\right) = -1 \rightarrow W_p\left(j\Omega_0\right) = -\frac{1}{N\left(a_0\right)} \tag{8}$$

where $N(a_0)$ is the value of the describing function (DF) of the modified relay at a_0. Let b be the hysteresis of the modified relay, where $b = |\beta e_{max}| = |-\beta e_{min}| = \beta a$, for any amplitude of oscillations, a. The general expressions for $N(a)$ and $-1/N(a)$ are given by:

$$\begin{aligned} N(a) &= \frac{4h}{\pi a}\sqrt{1-\left(\frac{b}{a}\right)^2} - j\frac{4h}{\pi a}\left(\frac{b}{a}\right) \\ &= \frac{4h}{\pi a}\left(\sqrt{1-\beta^2} - j\beta\right) \\ -\frac{1}{N(a)} &= -\frac{\pi a}{4h}\left(\sqrt{1-\beta^2} + j\beta\right) \\ \left|\frac{1}{N(a)}\right| &= \left|-\frac{\pi a}{4h}\right|\sqrt{\left(\sqrt{1-\beta^2}\right)^2 + (\beta)^2} = \frac{\pi a}{4h} \end{aligned} \tag{9}$$

$$\begin{aligned} \angle\left(-\frac{1}{N(a)}\right) &= \angle\left(-\frac{\pi}{4}\frac{a}{h}\right) + \angle\left(\left(\sqrt{1-\beta^2} + j\beta\right)\right) \\ \angle\left(-\frac{1}{N(a)}\right) &= -\pi + \tan^{-1}\frac{\beta}{\sqrt{1-\beta^2}} = -\pi + \sin^{-1}\beta \end{aligned} \tag{10}$$

Fig. 2 shows the Nyquist plots of $W_p(j\omega)$ and $-1/N(a)$. The plot of $-1/N(a)$ is a ray starting from the origin and extending in proportion with a, forming an angle $\psi = \sin^{-1}\beta$ with the negative real axis. The state of sustained oscillations is represented by the intersection of the two plots, occurring at frequency $\omega = \Omega_0$, and expressed mathematically as follows:

$$\left|W_p\left(j\Omega_0\right)\right| = \left|-\frac{1}{N\left(a_0\right)}\right| = \frac{\pi a_0}{4h} = \frac{1}{K_u} \tag{11}$$

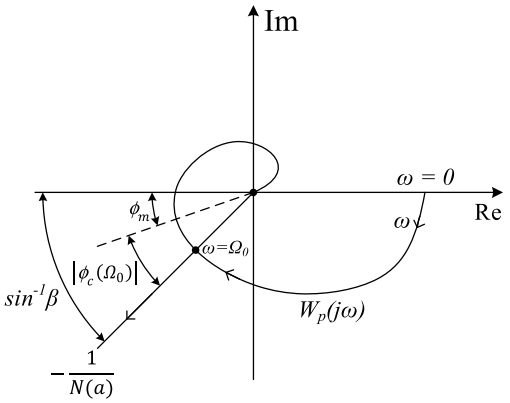

FIGURE 2. Nyquist plot of plant and the negative reciprocal of the relay's DF.

$$\angle W_p\left(\mathrm{j}\Omega_0\right) = \angle\left(-\frac{1}{N\left(a_0\right)}\right) = -\pi + \sin^{-1}\beta \tag{12}$$

The result in (11) is based on a substitution using first (9) then (6). Next, $W_c(j\omega)$ needs to be evaluated at the state of sustained oscillations (i.e. at Ω_0). The expression for $W_c(j\Omega_0)$ is given below, where (11) is used to substitute for K_u.

$W_c\left(\mathrm{j}\Omega_0\right) = K_c\left(1+\frac{1}{jT_i\Omega_0} + jT_d\Omega_0\right)$, or

$$\begin{aligned} W_c\left(\mathrm{j}\Omega_0\right) &= \frac{c_1}{\left|W_p\left(\mathrm{j}\Omega_0\right)\right|}\left(1+j\xi\right) \\ &= c_1K_u\left(1+j\left(2\pi c_3 - \frac{1}{2\pi c_2}\right)\right) \\ \left|W_c\left(\mathrm{j}\Omega_0\right)\right| &= \frac{c_1}{\left|W_p\left(\mathrm{j}\Omega_0\right)\right|}\sqrt{1+\xi^2} \end{aligned} \tag{13}$$

$$\angle W_c\left(\mathrm{j}\Omega_0\right) = \tan^{-1}\xi \tag{14}$$

It is recalled from basic control theory that phase margin is measured at the frequency where gain of the open-loop response, $|G_{ol}(j\omega)|$, is 1. The first criterion in (7) states that $c_1\sqrt{1+\xi^2} = 1$ is a condition for obtaining a phase margin of φ_m. Therefore, if at Ω_0 we have $|G_{ol}(\mathrm{j}\Omega_0)| = c_1\sqrt{1+\xi^2}$, then $|G_{ol}(\mathrm{j}\Omega_0)| = 1$ and the criterion is verified. Expressing $G_{ol}(\mathrm{j}\Omega_0)$ as a function of $W_p(\mathrm{j}\Omega_0)$ and $W_c(\mathrm{j}\Omega_0)$ results in the following:

$$\begin{aligned} G_{ol}\left(\mathrm{j}\Omega_0\right) &= W_c\left(\mathrm{j}\Omega_0\right) W_p\left(\mathrm{j}\Omega_0\right) \\ \rightarrow G_{ol}\left(\mathrm{j}\Omega_0\right) &= \frac{c_1}{\left|W_p\left(\mathrm{j}\Omega_0\right)\right|}\left(1+j\xi\right)\left|W_p\left(\mathrm{j}\Omega_0\right)\right| e^{j\angle W_p(\mathrm{j}\Omega_0)} \\ \rightarrow G_{ol}\left(\mathrm{j}\Omega_0\right) &= c_1\left(1+j\xi\right) e^{j\angle W_p(\mathrm{j}\Omega_0)} \\ \rightarrow \left|G_{ol}\left(\mathrm{j}\Omega_0\right)\right| &= c_1\sqrt{1+\xi^2} \end{aligned}$$

This proves the first criterion in (7). The second criterion in (7) is verified by considering the expression for $\angle G_{ol}(\mathrm{j}\Omega_0)$. Since it was established that Ω_0 is the frequency at which $|G_{ol}(\mathrm{j}\Omega_0)| = 1$, as a consequence $\angle G_{ol}(\mathrm{j}\Omega_0)$ should be $-\pi + \varphi_m$. Expressing $\angle G_{ol}(\mathrm{j}\Omega_0)$ in terms of $\angle W_p(\mathrm{j}\Omega_0)$ and $\angle W_c(\mathrm{j}\Omega_0)$ and using (12) and (14), the following is obtained:

$$\begin{aligned} \angle G_{ol}\left(j\Omega_0\right) &= \angle W_p\left(j\Omega_0\right) + \angle W_c\left(j\Omega_0\right) \\ \rightarrow -\pi + \phi_m &= \left(-\pi + \sin^{-1}\beta\right) + \tan^{-1}\xi \end{aligned}$$

Now the expression of β from the second criterion in (7) is substituted to finally verify the second criterion.

$-\pi+\phi_m = \left(-\pi + \sin^{-1}\sin\left(\phi_m - \tan^{-1}\xi\right)\right)+\tan^{-1}\xi = -\pi + \phi_m$

III. OPTIMIZING THE TEST PARAMETER β AND THE TUNING RULES

As mentioned earlier, the MRFT auto-tuning guarantees a specified phase margin provided the test parameter (β) and the tuning rules coefficients (c_1, c_2, c_3) satisfy the two criteria given in (7). But the MRFT auto-tuning can also be designed to provide near-optimal dynamic performance, as explained next. It is first noted that (7) has two conditions but four variables β, c_1, c_2, c_3. Therefore, two degrees of freedom exist in choosing these variables, and this is used to address the problem of optimizing the dynamic performance while still guaranteeing the desired phase margin. It is also worth noting that, as will be shown, this optimal selection is performed offline and once, i.e., it is not part of the online auto-tuning. In subsection *A*, the model of the dc-dc buck converter system that forms the basis of the optimization procedure is derived. In subsection *B,* a grid representing the range of dc-dc buck converter designs to which the developed MRFT auto-tuning can be applied is formed. Finally, the optimization procedure is detailed in subsection *C*.

A. MODEL OF DC-DC BUCK CONVERTER

A digitally controlled synchronous buck converter, operating in voltage-mode control, is considered for the implementation of the MRFT auto-tuning. The general schematic of such converter is given in Fig. 3. The output voltage (v_o) goes through a sensing circuit that includes an anti-aliasing filter. A resistive load (R_o) is assumed for this work. R_s is used to sense the inductor current (I_L) for protection purposes. In practical buck converters, ESR of the output capacitance is lowered by combining larger capacitor(s) that have a relatively higher ESR with smaller ceramic capacitor(s) that have a lower ESR. C_1 represents the larger capacitor(s), while C_2 represents the smaller capacitor(s). R_L, R_{C1}, and R_{C2} are the parasitic resistances of L, C_1, and C_2, respectively. The transfer function from d to v_o'' for the buck converter of Fig. 3, excluding the v_o sensing gain and excluding the anti-aliasing filter, is given in $G_{buck}(s)$, as shown at the bottom of the page, where C_o is the total output capacitance (including C_1 and C_2), R_C is the total capacitor ESR of C_o, and R_L' is the sum of the parasitic R_L, R_s, and the ON resistance of the conducting switch. τ represents the total delay in the system, and is given by $1.5T_s$, where sampling and control accounts for one sampling period (T_s) and triangular PWM accounts for $0.5T_s$.

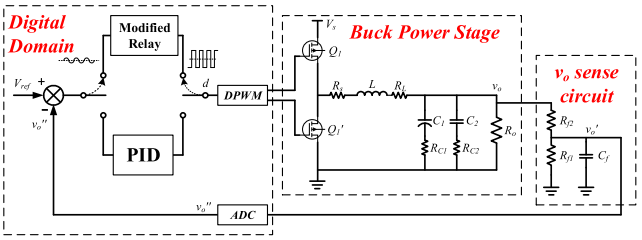

FIGURE 3. Schematic of the digitally-controlled dc-dc buck converter.

For the auto-tuning to be useful, it should be applicable to a wide range of converter designs, which may be represented by assigning a range to every variable in G_{buck}. But with so many variables in G_{buck}, a very large number of combinations exist, which would require a very lengthy optimization process. G_{buck} must therefore be simplified. The first simplification is to ignore the anti-aliasing filter, which is justifiable since its cutoff frequency is well above the buck converter dynamics. Constant scaling terms (such as V_s and the step-down gain of the v_o sensor) are removed, as they will be compensated for in the controller proportional gain. Next, assuming $R_o \gg R_L'$ and $R_o \gg R_C$, the terms $(1+R_L/R_o)$ and $(1+R_C/R_o)$ are approximated to 1; the product $R_C R_L'$ is very small and so can be approximated to 0.

The final and most significant simplification is related to total ESR (R_C). If high-ESR buck converters are considered, terms containing R_C cannot be neglected, and R_C should be treated as a variable in the TF and should be assigned a range. But in this work, for simplicity, only the case of low ESR is considered. As a result, the numerator ESR zero, as well as the term $C_o(R_C + R_L' + R_C R_L'/R_o)$ in the denominator's s-coefficient, may be eliminated. However, despite some simplifications of the model used for designing optimal tuning rules, the robustness is still present in this tuning due to the fulfillment of the phase margin constraints, which do not depend on the model used. The final simplified TF is given below:

$$G_{buck}(s) = \frac{e^{-\tau s}}{LC_o s^2 + \frac{L}{R_o}s + 1}$$

Let $T_1 = \sqrt{LC_o}$ and $T_2 = L/R_o$. G_{buck} is said to have three situational parameters, which are T_1, T_2, and τ. The situational parameters may be reduced to two through use of the scaled Laplace variable $s' = T_1 s$, which results in the TF below having only τ/T_1 and T_2/T_1 as situational parameters.

$$G_{buck}(S) = \frac{e - \frac{\tau}{T_1}S\prime}{S\prime^2 + \frac{T_2}{T_1}S\prime + 1} \tag{15}$$

$$G_{buck}(s) = e^{-\tau s}\frac{V_s\left(R_C C_o s+1\right)}{LC_o\left(1+\frac{R_C}{R_o}\right)s^2 + \left(C_o\left(R_C + R_L' + \frac{R_C R_L'}{R_o}\right) + \frac{L}{R_o}\right)s + \left(1+\frac{R_L'}{R_o}\right)}$$

B. GRID OF TFS REPRESENTING RANGE OF BUCK CONVERTER DESIGNS

In order to obtain a realistic range of TFs covering practical buck converter designs, basic component-sizing equations are utilized. The following equation may be used to size L in a buck converter [28]:

$$L = \frac{V_o(1-D)}{K_L I_o f_s},$$

where V_o and I_o are the nominal output voltage current, respectively. K_L is a coefficient related to the inductor current ripple that is typically set between 0.2 and 0.3 for a buck converter. $K_L = 0.3$ is chosen to get the minimum L, since L will be scaled up later. The nominal duty-cycle (D) is taken as 0.5. Noting that the ratio of V_o to I_o is equal to the load resistance (R_o), the minimum inductance (L_{min}) is given by:

$$L_{min} = \frac{0.5R_o}{0.3f_s} = \frac{5}{3}\frac{R_o}{f_s}. \tag{16}$$

The design criteria for C_o in case of low ESR is given below [28], [29], where K_{Co} is the desired maximum percent ripple in the output capacitor voltage.

$$C_o = \frac{1}{8f_s}\frac{K_L I_o}{K_{Co} V_o}$$

Taking K_C as 1%, the following expression is obtained for the minimum inductance, C_{o-min}:

$$C_{o-min} = \frac{1}{8f_s}\frac{0.3I_o}{0.01V_o} = \frac{15}{4}\frac{1}{f_s R_o} = \frac{3.75}{f_s R_o}. \tag{17}$$

Defining scaling factors α_L for L and α_C for C_o, and using (16) and (17), the situational parameters and thus the expression for G_{buck} in (15) may be rewritten as follows:

$$T_1 = \sqrt{LC_o} = \sqrt{\alpha_L L_{min}\alpha_C C_{o-min}} = \frac{5}{2}\frac{\sqrt{\alpha_L\alpha_C}}{f_s}$$

$$T_2 = \frac{L}{R_o} = \frac{\alpha_L L_{min}}{R_o} = \frac{5}{3}\frac{\alpha_L}{f_s}$$

$$\rightarrow \frac{\tau}{T_1} = \frac{0.6}{\sqrt{\alpha_L\alpha_C}} \text{ and } \frac{T_2}{T_1} = \frac{2}{3}\sqrt{\frac{\alpha_L}{\alpha_C}}$$

$$G_{buck}(S) = \frac{e - \left(\frac{0.6}{\sqrt{\alpha_L\alpha_c}}\right)S'}{s'^2 + \left(\frac{2}{s}\sqrt{\frac{\alpha_L}{\alpha_C}}\right)S' + 1} \tag{18}$$

Comparing the characteristic polynomial in the denominator of (18) to the standard second order system format of $(s^2 + 2\zeta\omega_n + \omega_n^2)$, the damping factor ζ is found to be $0.33\sqrt{\alpha_L}/\alpha_C$, while the natural frequency ω_n is 1. By considering all combinations of α_L and α_C from 1 to 10, a whole range of converters are represented. An illustration of this in grid format is provided in Fig. 4. Finally, to further justify the approximation of neglecting the ESR, its effect is represented to some extent by increasing the damping (ζ) in (18). This is done by making sure $\alpha_L \geq \alpha_C$, which results in ζ being ≥ 0.33. A total of 55 TFs (shown as shaded boxes in Fig. 4) are obtained after applying the criterion $\alpha_L \geq \alpha_C$. The TFs are numbered serially from 1 to 55, with the TF number appearing in the respective box in Fig. 4.

$\alpha_C \rightarrow$

$\alpha_L\downarrow$	1	2	3	4	5	6	7	8	9	10
1	1									
2	2	3								
3	4	5	6							
4	7	8	9	10						
5	11	12	13	14	15					
6	16	17	18	19	20	21				
7	22	23	24	25	26	27	28			
8	29	30	31	32	33	34	35	36		
9	37	38	39	40	41	42	43	44	45	
10	46	47	48	49	50	51	52	53	54	55

FIGURE 4. Grid of TFs representing the range of buck converter designs.

C. OBTAINING THE GLOBALLY OPTIMAL (β, c_1, c_2, c_3)

Obtaining optimal tuning rules can mathematically be formulated as the problem of optimization under uncertainty [30]. In the MRFT auto-tuning method, the globally optimal set of (β, c_1, c_2, c_3) is obtained using a two-stage optimization process, as suggested in [26], [31]. In the first stage, the optimal set of (β, c_1, c_2, c_3) for every TF in the grid of Fig. 4 is obtained through the optimization of the converter's dynamic performance in simulation, as further explained in subsection *C.1*. These are referred to as the locally optimal sets. The performance criterion used is the "integral of time weighted absolute error" (ITAE) – though any other time-domain or frequency-domain criterion, or a combination of them, may be used. The ITAE is calculated using (19), where $\boldsymbol{X}$ is the vector [β, c_1, c_2, c_3], t_0 is the time instant at which the transient occurs, and t_s is the settling time.

$$ITAE\ (\boldsymbol{X}) = \int_{t_0}^{t_0+t_s} (t-t_0)\,|e(t-t_0, \boldsymbol{X})|\,dt \tag{19}$$

In the second stage, one of the produced locally optimal sets of (β, c_1, c_2, c_3) is chosen to define global optimal tuning rules. This selection is done on the basis of least-worst performance relative to the locally optimal case, as explained in subsection *C.2* below. This is referred to as the "principle of least performance degradation", because the used tuning rule is optimal only for one specific set of converter parameters but is used for all converters. The numerical optimizations are performed using MATLAB and Simulink. Below is a detailed explanation of the two stages of the offline optimization:

C.1. Obtaining locally optimal (β, c_1, c_2, c_3) sets

Let G_{buck-n}, $n = 1$ to 55, represent the 55 TFs in the grid of Fig. 4. The locally optimal (β, c_1, c_2, c_3) set for each G_{buck-n} is obtained using an iterative procedure that utilizes the MATLAB *fminsearch* function – which is based on the Nelder-Mead simplex direct search algorithm [32]. Each iteration consists of the following 3 steps:

1. The test stage described by the block diagram of Fig. 1 (a), with $W_p(s) = G_{buck-n}$ and using the modified relay of (5), is simulated in Simulink using the initial/current β. T_u and a_0 obtained from the simulation are recorded.

2. PID controller coefficients are calculated from (3) using the T_u and a_0 from step 1 and the initial/current (c_1, c_2, c_3).
3. Using the PID controller obtained in step 2 and the current G_{buck-n}, a closed-loop simulation of a step in V_{ref} is performed and the ITAE is calculated using (19).

The *fminsearch* function updates the set (β, c_1, c_2, c_3) after every iteration of steps 1-3 to result in a lower ITAE. It is ensured at every iteration that the new (β, c_1, c_2, c_3) set still satisfies the constraints in (7). Iterations of steps 1-3 are repeated until the improvement in ITAE is below a specified tolerance. This is repeated for all the G_{buck-n}, $n = 1$ to 55. The final output of the first stage of the optimization is therefore a group of locally optimal sets (β^n, c_1^n, c_2^n, c_3^n) for $n = 1$ to 55, where each (β^n, c_1^n, c_2^n, c_3^n) results in the lowest ITAE for the corresponding G_{buck-n}.

C.2. Obtaining the globally optimal (β, c_1, c_2, c_3) set

The second stage of the optimization applies the principle of "least performance degradation" to obtain a globally optimal set of (β, c_1, c_2, c_3). This is done as follows:

1. Using β^1 (from the locally optimal set of G_{buck-1}), MRFT is simulated for G_{buck-1} to $G_{buck-55}$. Respective MRFT measurements,T_{u1^n} and a_{01^n} (for $n = 1$ to 55) are recorded.
2. Now using c_{1^1}, c_{2^1}, and c_{3^1} (from the locally optimal set of G_{buck-1}), along with $T_{u1}{}^n$ and a_{01^n} (for $n = 1$ to 55) from the previous step, a PID controller $C_{1^n}(s)$ is designed for each of G_{buck-1} to $G_{buck-55}$ using (3). Thus, $C_{1^n}(s)$ is based on G_{buck-_n} and the set (β^1, c_1^1, c_2^1, c_3^1) that is locally optimal to G_{buck-1}.
3. Next, each G_{buck-n} is simulated in closed-loop using its corresponding PID controller from the previous step, $C_1^n(s)$. For example: G_{buck-1} and $C_{1^1}(s)$, G_{buck-2} and $C_{1^2}(s)$, and so on are simulated. Each time the corresponding ITAE, denoted ITAE_{1^n} (for $n = 1$ to 55) is recorded. The single maximum (worst-case) ITAE, ITAE_{1^n}, is then found.
4. Steps 1, 2, and 3 are repeated using (β^2, c_{1^2}, c_{2^2}, c_{3^2}) to obtain ITAE_2^n for $n = 1$ to 55, and ITAE_2^n is recorded. This is repeated until all worst-case ITAEs, ITAE_{k^n} for $k = 1$ to 55, are recorded.

The globally optimal set, (β^*, c_1^*, c_2^*, c_3^*), is the set with the lowest $\max_{n=1,2,\ldots 55} \text{ITAE}_{k^n}$. In other words, it is the set that results in the least performance degradation when applied to all converters in the considered range. This completes the second and final stage of the optimization.

The two-stage optimization process described above was carried out on a PC with an Intel Core i7-4700MQ 2.40 GHz CPU and 16 GB RAM, and it took about five hours to complete. Constraints used include restricting ϕ_m in (7) to the range [20°, 60°], restricting c_2 to [0.1, 100], and considering only positive values for c_1 and c_3. Another constraint was to consider only $\beta \geq -0.2$, since large negative values of β result in MRFT oscillations of higher frequency, whereas it is desired to have a lower MRFT frequency in order to get more ADC samples per cycle of MRFT oscillation – which enables higher accuracy. The set (β^3, c_1^3, c_2^3, c_3^3) was found to result in the least performance degradation among all sets, and is thus taken as the globally optimal set; it resulted in a phase margin of $\phi_m = 35°$, and had the following numerical values:

$$\beta^* = -0.2, \quad c_1^* = 0.69, \quad c_2^* = 1.14, \quad c_3^* = 0.19. \quad (20)$$

In other words, using the coefficients in (20) to tune a controller for every other G_{buck-n} system in the considered range resulted in the least performance degradation from the locally optimal performance, ITAE_3^3. The worst-case ITAE, expressed as $\max_{n=1,2,\ldots 55} \text{ITAE}_3^n$, was found to be only 13% greater than the locally optimal case ITAE_3^3.

IV. EXPERIMENTAL RESULTS

A dc-dc buck converter prototype similar to that depicted in Fig. 3 is used for experimental verification. A TMS320F28335 digital microcontroller is utilized; the PWM frequency is set to 200 kHz, and the sampling rate is also set to 200 KHz and is synchronized with the PWM. R_o can be electronically switched between two values to provide load transients for controller testing. Nominal input supply voltage (V_s) is 9 V while the reference output voltage (V_{ref}) is 2 V. Four different combinations of L and C_1 are used in the experiments to provide different test cases for the MRFT auto-tuning. The values considered for L are 4.8 μH and 10 μH. Capacitance C_1 consists of two parallel Aluminum-polymer (low-ESR) capacitors; the values used are 2 x 220 μF and 2 x 330 μF. Capacitance C_2 is made of three parallel 22 μF ceramic capacitors and it is not changed.

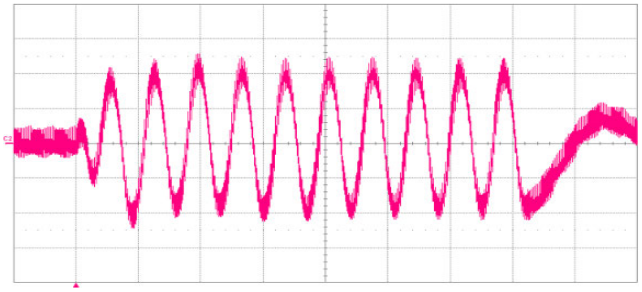

FIGURE 5. Experimental MRFT oscillations in v_o (20 mV/div, 200 μs/div).

A. MRFT AUTO-TUNING OF THE PID CONTROLLER

A.1. Step 1 of MRFT Auto-tuning: Test Stage

Auto-tuning is initiated upon the user's command, though it can also be programmed to run according to a schedule or based on an event. MRFT auto-tuning is first demonstrated using the combination $L = 4.8$ μH and $C_1 = 2$ x 220 μF. Using the value of β from (20), the MRFT is run and experimentally measured oscillations (in v_o) are shown in Fig. 5; a short transient of around two cycles is followed by steady MRFT oscillations. These oscillations are captured by the ADC, and the microcontroller measures T_u and a_0 as an average over all oscillation cycles – excluding the short initial transient of one or two cycles. This concludes the test stage.

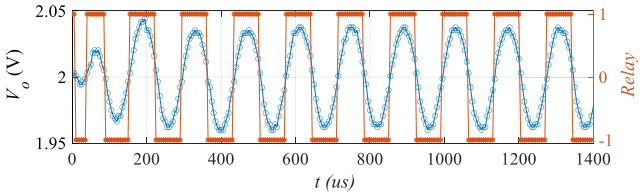

FIGURE 6. Experimental MRFT oscillations (blue) and relay status (red).

A.2. Step 2 of MRFT Auto-tuning: Tuning Stage

The tuning stage is automatically started right after the completion of the test stage, and it is simply to compute the new PID controller coefficients from (3) using the measured a_0 and T_u and using the (c_1, c_2, c_3) from (20). K_u is obtained using (6). T_u came out to be 138 μs while K_u was 11.4 V^{-1}. This concludes the short and practical MRFT auto-tuning. The result is a PID controller that guarantees a phase margin of 35° and produces near-optimal transient performance.

Before the evaluation and discussion of the performance of the auto-tuned controller, some notes on the auto-tuning process itself are made. Fig. 6 shows the MRFT oscillations as captured by the ADC, which are recorded in microcontroller memory as contiguous ADC samples. Also shown in Fig. 6 is a plot of the relay's output, where +1 (relay ON) indicates that the output of the relay block is $D + h$, while −1 (relay OFF) indicates that the output of the relay block is $D - h$. The v_o ADC samples are marked by blue circles whereas the relay status samples are shown as red stars. It is noted that the sampled v_o signal of Fig. 6 does not contain switching ripple, which allows for accurate measurement of a_0 and T_u by the controller. Absence of the switching ripple is attributed to the filtering provided by the anti-aliasing LPF, as well as due to the sampling being synchronized with the PWM. It is also noted from Fig. 5 that the amplitude of the MRFT oscillations is relatively low, being $< \pm 0.045$ V around the nominal 2 V (i.e., ∼2%). This is because in the proposed MRFT auto-tuning, oscillations are excited at a frequency corresponding to a phase angle of $-(180° - \sin^{-1}\beta) = -191.54°$ (i.e. $\beta = -0.2$), which is well after the LC resonant frequency that occurs around −90°. The gain (from d to v_o) at this point is quite low, resulting in moderate oscillations, which is an advantage of the MRFT auto-tuning over methods such as [9], [10] which excite oscillations at the LC resonant frequency. Another advantage noted from Fig. 5 is that oscillations last only for a short duration. The whole test lasts for around 1.7 ms, which includes about 9 stable oscillation cycles, plus the short initial and final transients. If desired, the test may be further shortened by using less cycles. For example, if only 5 stable cycles are used, the test duration would only be about 1 ms.

B. PERFORMANCE OF THE MRFT AUTO-TUNED CONTROLLER

Two tests are conducted with the MRFT auto-tuned PID controller. First, a step in V_{ref} from 2 V to 2.2 V is applied; results are shown in Fig. 7(a). The overshoot in v_o is less than 4% of the steady-state 2.2 V. In the second test, a step in the output current (i_o) from 0.27 A to 1.27 A is applied; the resulting waveforms are shown in Fig. 7 (b). The undershoot in v_o is around 7%. Both results represent satisfactory performance for the MRFT auto-tuned controller, especially that this first test setup used conservative values $L = 4.8$ μH and $C_1 = 2$ x 220 μF, which provided low damping.

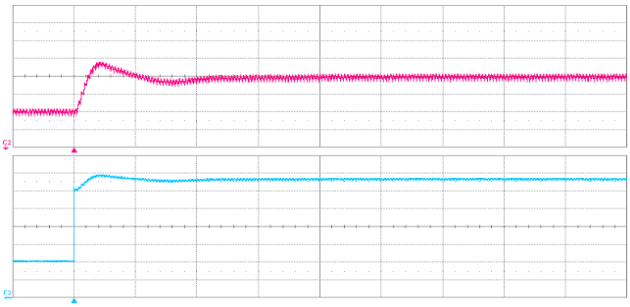

(a) Step in V_{ref} from 2.0 V → 2.2 V (100 µs/div)

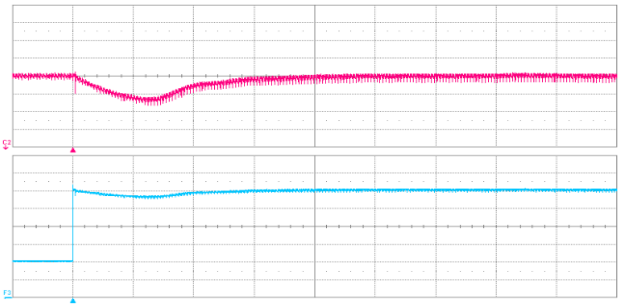

(b) Step in load (i_o) from 0.27 A → 1.27 A (100 µs/div)

FIGURE 7. Responses of v_o (pink, 100 mV/div) and i_o (blue, 0.25 A/div).

TABLE 1. PID Controller Parameters for MRFT Auto-Tuned and Optimal Controllers for all four Experimental Designs.

Design #		Controller Type	K_c	Ti (µs)	T_d (µs)
1	$L = 10$ µH, $C_1 = 660$ µF	MRFT auto-tuned	10.5	150	25
		Optimal non-auto	7.3	193	36
2	$L = 10$ µH, $C_1 = 440$ µF	MRFT auto-tuned	7.9	157	26
		Optimal non-auto	5.6	145	35
3	$L = 4.8$ µH, $C_1 = 660$ µF	MRFT auto-tuned	4.6	100	17
		Optimal non-auto	4.8	132	16
4	$L = 4.8$ µH, $C_1 = 440$ µF	MRFT auto-tuned	3.7	96	16
		Optimal non-auto	4.3	105	16

C. MRFT AUTO-TUNING FOR SEVERAL CONVERTER DESIGNS

In order to show the versatility of the MRFT auto-tuning, it is tested on four different buck converter designs made with the different L and C_1 combinations described earlier. The MRFT auto-tuning is run on each design, and the resulting PID controller coefficients are given in Table 1. To better judge the performance of the MRFT auto-tuned controllers,

TABLE 2. Phase Margin (PM) in degrees, Gain Margin (GM) in dB, and Bandwidth (BW) in kHz obtained with MRFT Auto-Tuned and Optimal Controllers.

Design #		Controller Type	PM	GM	BW
1	$L = 10$ µH, $C_1 = 660$ µF	MRFT auto-tuned	28.8	12.4	14.2
		Optimal non-auto	41.2	13.1	13.6
2	$L = 10$ µH, $C_1 = 440$ µF	MRFT auto-tuned	28.9	11.3	13.6
		Optimal non-auto	38.7	12.8	14.1
3	$L = 4.8$ µH, $C_1 = 660$ µF	MRFT auto-tuned	37.5	17.1	15.5
		Optimal non-auto	37.4	17.1	15.8
4	$L = 4.8$ µH, $C_1 = 440$ µF	MRFT auto-tuned	37.8	16.5	16.1
		Optimal non-auto	37.6	15.1	18.5

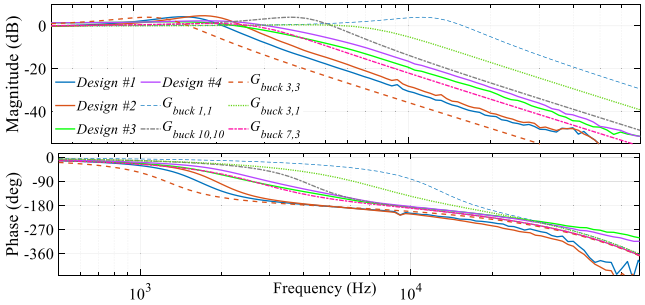

FIGURE 8. Measured frequency response of the four buck converter designs along with Bode plots of G_{buck} for various combinations of α_L and α_C.

a manually-tuned optimal controller is used for comparison. The procedure used to design this "optimal controller" is as follows. For each converter design, experimentally measured FR data is first obtained with the aid of the Texas Instruments Software Frequency Response Analyzer (SFRA) tool [33]. A high order TF is fitted to this FR data, and the TF is used to simulate the response to a V_{ref} step. A controller that gives the lowest ITAE is obtained through an optimization with MATLAB's *fminsearch*. It is noted that this optimal controller differs from the MRFT auto-tuned controller in that it is optimized only for the given converter design and cannot be re-tuned to other converters, and that it does not guarantee a specific gain or phase margin. So while the optimal controller is expected to perform better, it is not practically feasible as it requires an identification followed by a software optimization for every converter that is manufactured. MRFT auto-tuning on the other hand requires neither an identification nor an online optimization. The PID controller coefficients of the optimal controller for each of the four converter designs are also given in Table 1 alongside the PID coefficients of the MRFT auto-tuned controllers.

D. PLANT AND OPEN-LOOP BODE PLOTS FOR ALL DESIGNS

Fig. 8 shows the measured frequency responses (FR) of the four converter designs obtained using the SFRA tool

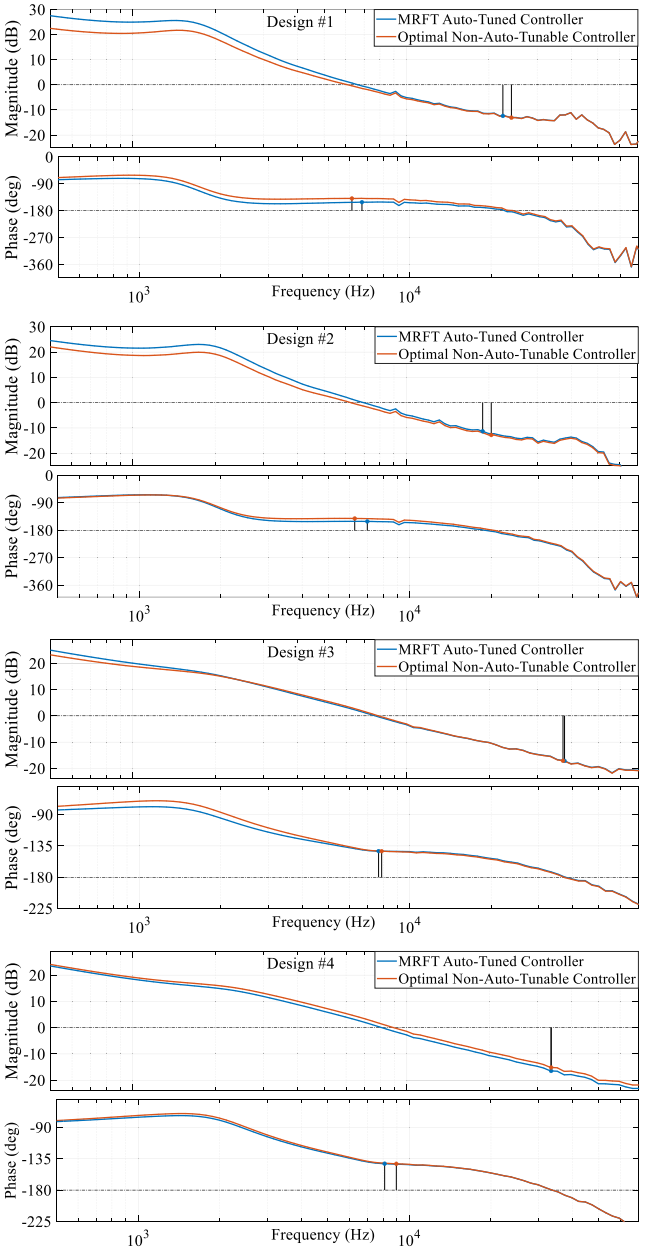

FIGURE 9. Open-loop responses for the four buck converter designs using the experimentally measured plant responses and the designed PID controllers.

(solid lines), and also gives Bode plots of the analytical model (G_{buck}) for a few combinations of α_L and α_C (dashed lines) – but using G_{buck} with the regular s and not the scaled s' to allow for direct comparison with the measured FRs of the converters. Fig. 8 illustrates the wide range covered by the grid of Fig. 4. For example, with $\alpha_L = 1$ and $\alpha_C = 1$, the resonance is above 10 kHz, while at the other extreme with $\alpha_L = 10$ and $\alpha_C = 10$, the resonance is just above 1 kHz. Intermediate frequencies with different levels of damping are shown as well. It is also noted that the measured FRs of the four experimental designs lie well within the range defined by the grid – with the exception that experimentally measured FRs show excess phase lag at higher frequencies.

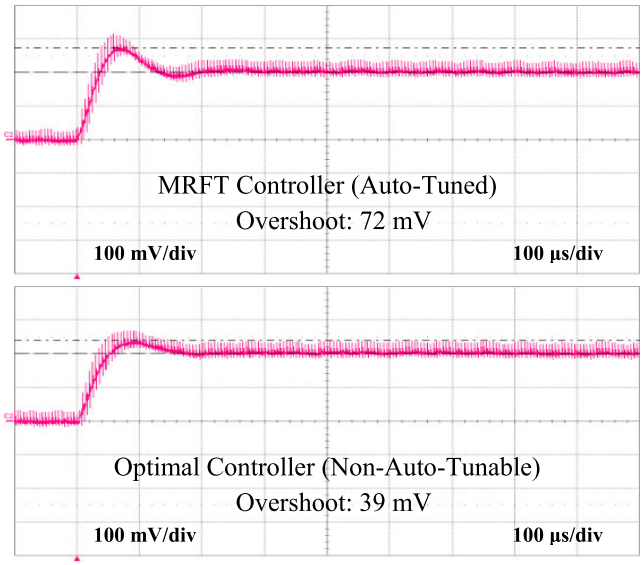

FIGURE 10. Design #1 (10 μH, 660 μF): v_o response for 2V→2.2 V step in V_{ref}.

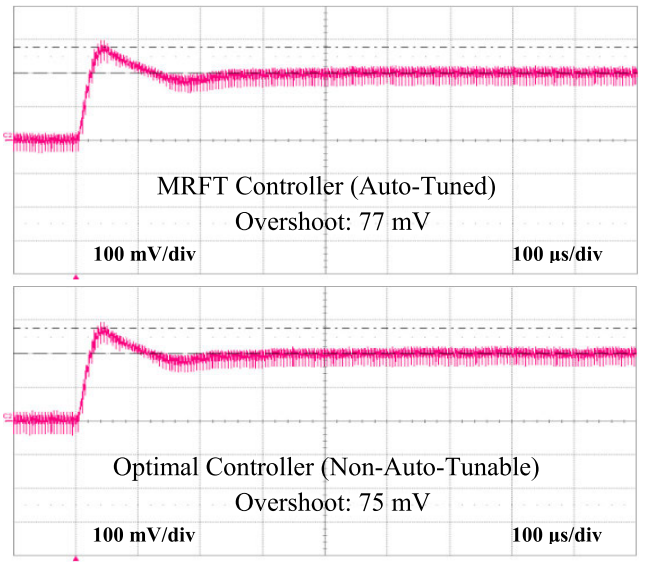

FIGURE 12. Design #3 (4.8 μH, 660 μF): v_o response for 2V→2.2 V step in V_{ref}.

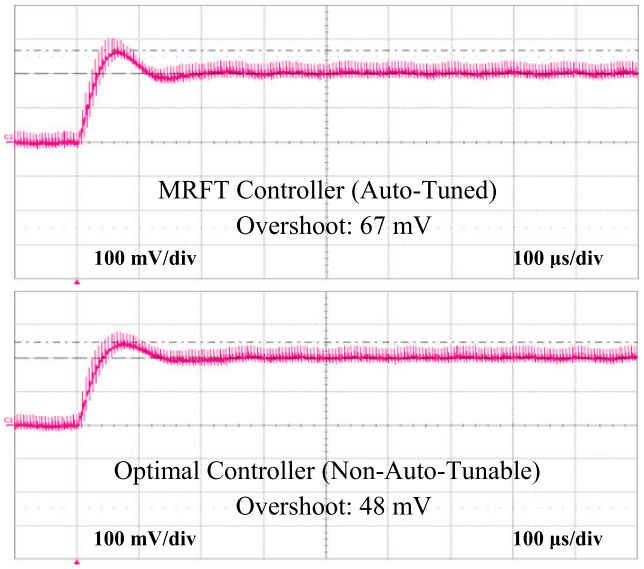

FIGURE 11. Design #2 (10 μH, 440 μF): v_o response for 2V→2.2 V step in V_{ref}.

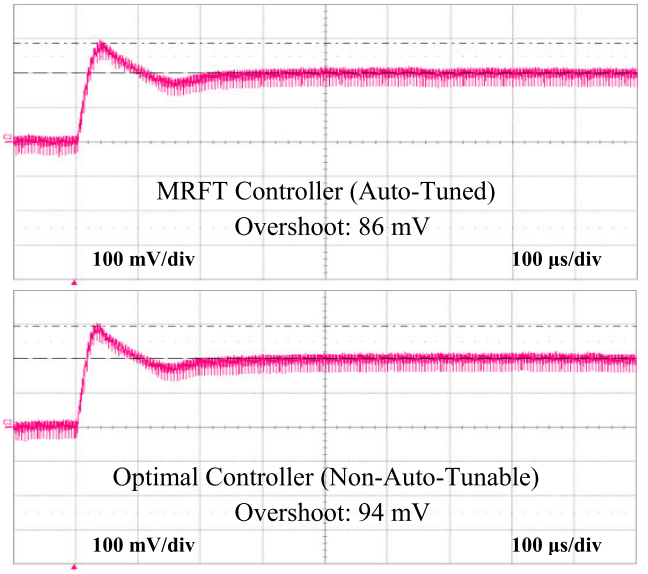

FIGURE 13. Design #4 (4.8 μH, 440 μF): v_o response for 2V→2.2 V step in V_{ref}.

Next, Bode plots of the open-loop responses (based on the measured converter FRs and the designed controllers), are shown in Fig. 9. Gain/phase margins are extracted for the four converter designs and given in Table 2. The bandwidth is obtained using the corresponding closed-loop FR data and is also given in Table 2. It is seen from Table 2 that the phase margin obtained by MRFT auto-tuned controllers in designs 3 and 4 is only about 3° above the designed value of 35°, while for designs 1 and 2 it is only 6° less than 35°. These offsets from the specified phase margin are attributed to minor errors in the measurement of T_u and a_0, and the small inaccuracy in applying the designed hysteresis (βa_0) due to limited number of samples per cycle of MRFT oscillation. The optimal controller has similar phase margin for designs 3 and 4 but is better in designs 1 and 2. As for gain margin and bandwidth, MRFT and optimal controllers are quite close in all cases. This is expected since both controllers share the same design objective of minimizing ITAE following a step in V_{ref} – but with the major difference that in MRFT auto-tuning this is achieved through a simple auto-tuning process that can be performed on any converter, whereas the optimal controller only applies to the specific converter and requires a lengthy design process.

E. PERFORMANCE COMPARISON FOR ALL FOUR DESIGNS

Finally, experimental results for the dynamic performance of the MRFT and optimal controllers are given in Figures 10-17. Figures 10-13 provide results for a step change in V_{ref}.

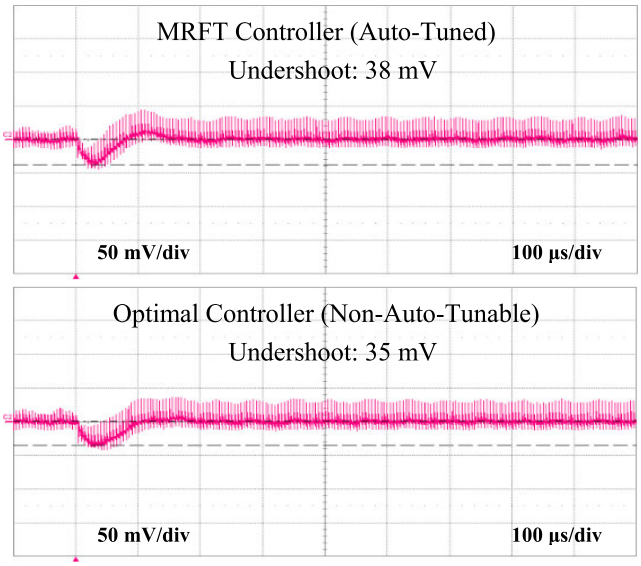

FIGURE 14. Design #1 (10 μH, 660 μF): v_o response for 0.27A→1.27A i_o step.

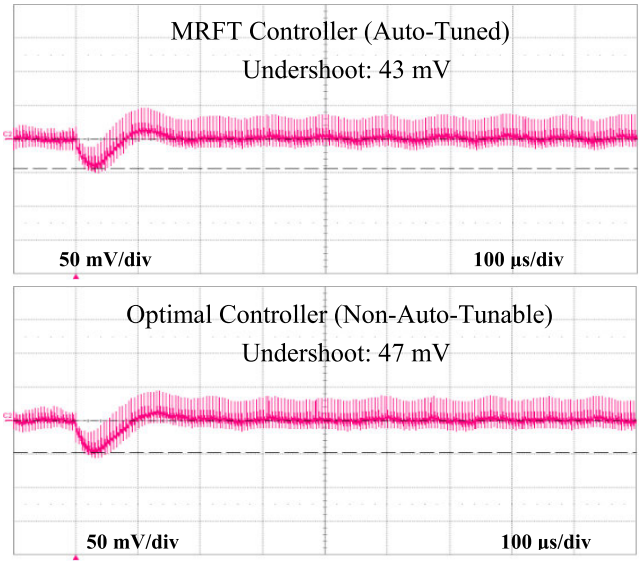

FIGURE 15. Design #2 (10 μH, 440 μF): v_o response for 0.27A→1.27A i_o step.

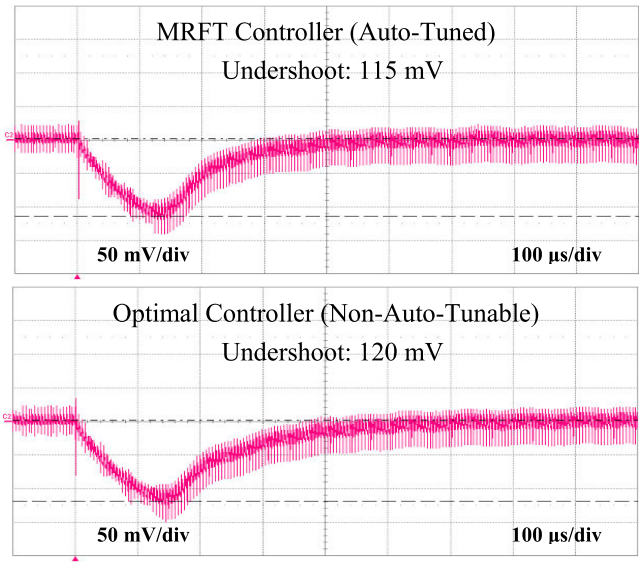

FIGURE 16. Design #3 (4.8 μH, 660 μF): v_o response for 0.27A→1.27A i_o step.

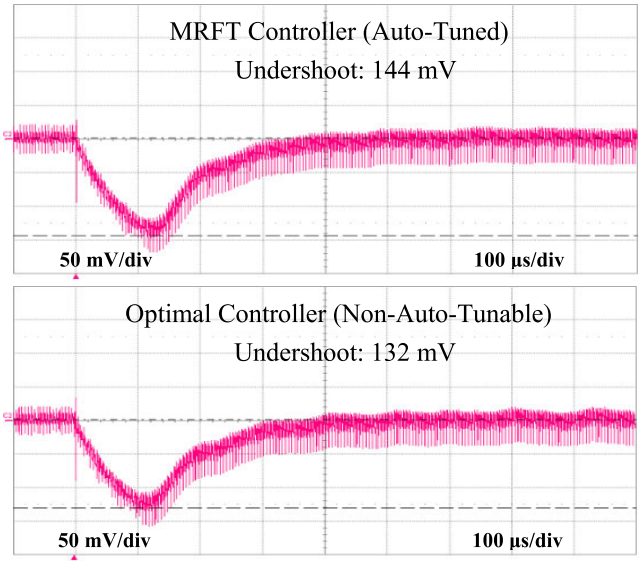

FIGURE 17. Design #4 (4.8 μH, 440 μF): v_o response for 0.27A→1.27A i_o step.

The overshoot of the MRFT auto-tuned controller is larger than that of the optimal controller for three of the designs but is lower for one design. Settling times are very similar for all designs. This is expected, since the optimal controller is designed for the specific converter using full knowledge of the converter's FR. But while the optimal controller is non-auto-tunable, the MRFT controller can be retuned upon any change in the system's parameters or operating point. Figures 14-17 provide results for a step change in the load. The MRFT auto-tuned controller performs equally well as the optimal, and in some cases even better. This is not unexpected, since the optimal controller is designed to perform optimally for a step in V_{ref} and not a step in I_o. To summarize, the overall performance of the MRFT auto-tuned controller is quite satisfactory in all designs, and so is expected to perform well in any buck converter design.

V. CONCLUSION

This paper presents the design and implementation of the MRFT auto-tuning method applied to a digitally-controlled dc-dc buck converter. MRFT auto-tuning is simple and reliable; it consists of short and simple test and tuning stages and does not require any knowledge of the converter or load parameters. The main contribution of the this work is the design of the MRFT auto-tuning for the class of dc-dc buck converters by selecting the test stage parameter (β) and the coefficients of the tuning rules (c_1, c_2, c_3) through a two-stage optimization process, with the objective of producing a controller that provides near-optimal dynamic performance for

a converter randomly picked from a wide range of dc-dc buck converter designs. To verify the MRFT auto-tuning method with the designed set of (β, c_1, c_2, c_3), experimental results for the auto-tuning on four different buck converter designs are provided. The results show good performance of the designed controllers, even though no prior knowledge of the converter or load parameters is used. Mathematical proof that the specified phase margin is guaranteed by the MRFT auto-tuning method is also provided in the paper. The simplicity and short duration of the MRFT auto-tuning, along with its ability to provide near-optimal dynamic performance, makes it a viable option for the auto-tuning of digitally-controlled converters. Suggested future work includes applying the MRFT auto-tuning method to other types of converters and loads, which requires the design (optimization) of new tuning rules.

REFERENCES

[1] D. Maksimovic, R. Zane, and R. Erickson, "Impact of digital control in power electronics," in *Proc. 16th Int. Symp. Power Semiconductor Devices (IC's)*, Kitakyushu, Japan, 2004, pp. 13–22.

[2] B. Miao, R. Zane, and D. Maksimović, "Automated digital controller design for switching converters," in *Proc. IEEE 36th Conf. Power Electron. Spec. (PESC)*, Recife, Brazil, 2005, pp. 2729–2735.

[3] M. Shirazi, R. Zane, D. Maksimović, L. Corradini, and P. Mattavelli, "Autotuning techniques for digitally-controlled point-of-load converters with wide range of capacitive loads," in *Proc. 22nd Annu. IEEE Appl. Power Electron. Conf. Expo. (APEC)*, Anaheim, CA, USA, Feb. 2007, pp. 14–20.

[4] M. Shirazi, R. Zane, and D. Maksimović, "An autotuning digital controller for DC–DC power converters based on online frequency-response measurement," *IEEE Trans. Power Electron.*, vol. 24, no. 11, pp. 2578–2588, Nov. 2009.

[5] A. Barkley and E. Santi, "Improved online identification of a DC–DC converter and its control loop gain using cross-correlation methods," *IEEE Trans. Power Electron.*, vol. 24, no. 8, pp. 2021–2031, Aug. 2009.

[6] A. Barkley, R. Dougal, and E. Santi, "Adaptive control of power converters using digital network analyzer techniques," in *Proc. 26th Annu. IEEE Appl. Power Electron. Conf. Expo. (APEC)*, Fort Worth, TX, USA, Mar. 2011, pp. 1824–1832.

[7] M. Bhardwaj, S. Choudhury, R. Poley, and B. Akin, "Online frequency response analysis: A powerful plug-in tool for compensation design and health assessment of digitally controlled power converters," *IEEE Trans. Ind. Appl.*, vol. 52, no. 3, pp. 2426–2435, May 2016.

[8] A. Shehada, Y. Yan, A. R. Beig, and I. Boiko, "Comparison of relay feedback tuning and other tuning methods for a digitally controlled buck converter," in *Proc. 45th Annu. Conf. IEEE Ind. Electron. Soc. (IECON)*, Lisbon, Portugal, Oct. 2019, pp. 1647–1652.

[9] W. Stefanutti, P. Mattavelli, S. Saggini, and M. Ghioni, "Autotuning of digitally controlled DC–DC converters based on relay feedback," *IEEE Trans. Power Electron.*, vol. 22, no. 1, pp. 199–207, Jan. 2007.

[10] L. Corradini, P. Mattavelli, and D. Maksimović, "Robust relay-feedback based autotuning for DC-DC converters," in *Proc. IEEE Power Electron. Spec. Conf. (PESC)*, Orlando, FL, USA, Jun. 2007, pp. 2196–2202.

[11] Z. Zhao and A. Prodic, "Limit-cycle oscillations based auto-tuning system for digitally controlled DC–DC power supplies," *IEEE Trans. Power Electron.*, vol. 22, no. 6, pp. 2211–2222, Nov. 2007.

[12] M. Faraji-Niri and A. Shaheydari, "Autotuing a PID controller for DC-DC buck converter by improved relay feedback test," in *Proc. IEEE 1st Int. Conf. New Res. Achievements Elect. Comput. Eng. (ICNRAECE)*, May 2016, pp. 1–6.

[13] K. Venkata Ramana, S. Majhi, and A. K. Gogoi, "Modeling and estimation of DC–DC buck converter dynamics using relay feedback output with performance evaluation," *IEEE Trans. Circuits Syst. II, Exp. Briefs*, vol. 66, no. 3, pp. 427–431, Mar. 2019.

[14] J. Morroni, R. Zane, and D. Maksimović, "Design and implementation of an adaptive tuning system based on desired phase margin for digitally controlled DC–DC converters," *IEEE Trans. Power Electron.*, vol. 24, no. 2, pp. 559–564, Feb. 2009.

[15] J. Morroni, L. Corradini, R. Zane, and D. Maksimović, "Adaptive tuning of switched-mode power supplies operating in discontinuous and continuous conduction modes," *IEEE Trans. Power Electron.*, vol. 24, no. 11, pp. 2603–2611, Nov. 2009.

[16] L. Corradini, P. Mattavelli, W. Stefanutti, and S. Saggini, "Simplified model reference-based autotuningfor digitally controlled SMPS," *IEEE Trans. Power Electron.*, vol. 23, no. 4, pp. 1956–1963, Jul. 2008.

[17] A. Costabeber, P. Mattavelli, S. Saggini, and A. Bianco, "Digital autotuning of DC–DC converters based on a model reference impulse response," *IEEE Trans. Power Electron.*, vol. 26, no. 10, pp. 2915–2924, Oct. 2011.

[18] S. Moon, L. Corradini, and D. Maksimović, "Autotuning of digitally controlled boost power factor correction rectifiers," *IEEE Trans. Power Electron.*, vol. 26, no. 10, pp. 3006–3018, Oct. 2011.

[19] J. A. A. Qahouq and V. Arikatla, "Online closed-loop autotuning digital controller for switching power converters," *IEEE Trans. Ind. Electron.*, vol. 60, no. 5, pp. 1747–1758, May 2013.

[20] S. Kapat, "Near time optimal PID tuning in a digitally controlled synchronous buck converter," in *Proc. IEEE 15th Workshop Control Modeling Power Electron. (COMPEL)*, Santander, Spain, Jun. 2014, pp. 1–8.

[21] A. L. Kelly and K. Rinne, "A self-compensating adaptive digital regulator for switching converters based on linear prediction," in *Proc. 21st Annu. IEEE Appl. Power Electron. Conf. Expo. (APEC)*, Dallas, TX, USA, Mar. 2006, pp. 712–718.

[22] M. Algreer, M. Armstrong, and D. Giaouris, "Adaptive PD+I control of a switch-mode DC–DC power converter using a recursive FIR predictor," *IEEE Trans. Ind. Appl.*, vol. 47, no. 5, pp. 2135–2144, Sep./Oct. 2011.

[23] M. Al-Greer, M. Armstrong, M. Ahmeid, and D. Giaouris, "Advances on system identification techniques for DC–DC switch mode power converter applications," *IEEE Trans. Power Electron.*, vol. 34, no. 7, pp. 6973–6990, Jul. 2019.

[24] K. J. Åström and T. Hägglund, "Automatic tuning of simple regulators with specifications on phase and amplitude margins," *Automatica*, vol. 20, no. 5, pp. 645–651, Sep. 1984.

[25] I. M. Boiko, "Loop tuning with specification on gain and phase margins via modified second-order sliding mode control algorithm," *Int. J. Syst. Sci.*, vol. 43, no. 1, pp. 97–104, Jan. 2012.

[26] I. Boiko, "Modified relay feedback test (MRFT) and tuning of PID controllers," in *Non-Parametric Tuning of PID Controllers: A Modified Relay-Feedback-Test Approach*. London, U.K.: Springer, 2013.

[27] D. P. Atherton, "Relay autotuning: An overview and alternative approach," *Ind. Eng. Chem. Res.*, vol. 45, no. 12, pp. 4075–4080, Jun. 2006.

[28] M. K. Kazimierczuk, "Buck PWM DC-DC converter," in *Pulse-Width Modulated DC-DC Power Converters*, 2nd ed. Chechester, U.K.: Wiley, 2015.

[29] S. P. Singh, "Output ripple voltage for buck switching regulator," Texas Instrum., Dallas, TX, USA, App. Rep. SLVA630A, 2014.

[30] A. Ben-Tal and A. Nemirovski, "Robust convex optimization," *Math. Oper. Res.*, vol. 23, no. 4, pp. 769–805, 1998.

[31] I. Boiko, "Design of non-parametric process-specific optimal tuning rules for PID control of flow loops," *J. Franklin Inst.*, vol. 351, no. 2, pp. 964–985, Feb. 2014.

[32] J. C. Lagarias, J. A. Reeds, M. H. Wright, and P. E. Wright, "Convergence properties of the Nelder–Mead simplex method in low dimensions," *SIAM J. Optim.*, vol. 9, no. 1, pp. 112–147, Jan. 1998.

[33] *C2000 Software Frequency Response Analyzer (SFRA) Library and Compensation Designer in SDK Framework*, Texas Instrum., Dallas, TX, USA, 2018.

AHMED SHEHADA received the B.Eng. degree (Hons.) from McGill University, Montreal, Canada, in 2003, the M.Sc. degree from The Petroleum Institute (now Khalifa University), Abu Dhabi, United Arab Emirates, in 2010, and the Ph.D. degree from Virginia Tech, Blacksburg, VA, in 2017, all in electrical engineering. He was an Intern for two short periods in 2013 and 2014 at Regal Beloit America, Blacksburg, where he worked on converters for switched reluctance motor drives. He is currently a Postdoctoral Fellow with the Department of Electrical Engineering and Computer Science, Khalifa University. His research interests include control in power electronics and electric motor drives, and multilevel power electronic converters.

YAN YAN received the B.Eng. degree from Beijing Jiaotong University, China, in 2011, and the M.Sc. degree from Khalifa University, Abu Dhabi, United Arab Emirates, in 2019, all in electrical engineering. From 2011 to 2015, he was a Control Engineer with China Southern Power Grid Company Ltd (CSG). He was also a Research Associate with the Department of Electrical Engineering and Computer Science, Khalifa University, from 2019 to 2020. He is currently a Design Engineer focusing on solar plants at Powerchina Huadong Engineering Corporation Ltd., Dubai. His research interests include modular multi-level converters and auto-tuning of power electronic converters.

ABDUL R. BEIG (Senior Member, IEEE) received the B.Eng. degree in electrical and electronics engineering from the National Institute of Technology, Karnataka, Surathkal, India, in 1989, and the M.Tech. and Ph.D. degrees in electrical engineering from the Indian Institute of Science, Bengaluru, India, in 1998 and 2004, respectively. He is currently an Associate Professor with the Advanced Power and Energy Center, Department of Electrical Engineering and Computer Science, Khalifa University, Abu Dhabi, United Arab Emirates. His current research interests include high-gain converters, auto-tuning of grid connected converters, electric vehicles, modular multilevel converters, and SiC-based converters. He has been serving as an Associate Editor for the IEEE TRANSACTIONS ON INDUSTRY APPLICATIONS.

IGOR BOIKO (Senior Member, IEEE) received the M.Sc., Ph.D., and D.Sc. (Habil.) degrees in electromechanical engineering and control system engineering. He is currently a Professor with the Department of Electrical Engineering and Computer Science, Khalifa University of Science and Technology, Abu Dhabi, United Arab Emirates. His research interests include discontinuous control, sliding mode control, power converter control, robotics, frequency-domain methods, and PID controller tuning. In particular, he developed such methods and concepts as the LPRS method, dynamic harmonic balance, phase deficit, fractal dynamics, and optimal non-parametric controller tuning. He has authored/coauthored four books and a number of journals and conference papers. He is a member of the IEEE Technical Committee on Variable Structure Systems.